

Measuring the complex admittance of a carbon nanotube double quantum dot

S.J. Chorley,¹ J. Wabnig,¹ Z.V. Penfold-Fitch,¹ K.D. Petersson,^{1,*} J. Frake,¹ C.G. Smith,¹ and M.R. Buitelaar^{1,†}

¹*Cavendish Laboratory, University of Cambridge, Cambridge CB3 0HE, United Kingdom*

We investigate radio-frequency (rf) reflectometry in a tunable carbon nanotube double quantum dot coupled to a resonant circuit. By measuring the in-phase and quadrature components of the reflected rf signal, we are able to determine the complex admittance of the double quantum dot as a function of the energies of the single-electron states. The measurements are found to be in good agreement with a theoretical model of the device in the incoherent limit. Besides being of fundamental interest, our results present an important step forward towards non-invasive charge and spin state readout in carbon nanotube quantum dots.

PACS numbers: 73.63.Fg, 73.63.Kv, 73.23.Hk, 03.67.Lx

An important requirement in any quantum information processing scheme is fast manipulation and readout of the quantum system in which the quantum information is encoded. This requires an understanding of the response of the quantum system at finite frequencies which, in the case of an electronic device, involves an understanding of its complex admittance [1, 2]. Of particular interest in the context of quantum information processing are double quantum dots which are widely used to define charge and spin qubits [3]. However, while double quantum dots have been investigated in detail over the last decade, experiments to measure and analyze their complex admittance have not yet been performed and this topic has only recently been addressed theoretically [4]. The admittance of quantum dots at finite frequencies is non-trivial as exemplified by recent experiments on single quantum dots [5, 6]. The physics is even richer for double quantum dots as internal charge dynamics, i.e. charge transfer between the quantum dots, has to be taken into account. However, the dependence of the admittance on the internal charge dynamics also provides a route towards charge and spin state readout [7].

In this work we present a detailed experimental study of the complex admittance of a carbon nanotube double quantum dot which is measured using rf reflectometry techniques. The measurements are compared with a theoretical model of the device where we use a density matrix approach to calculate the double quantum dot admittance. The good quantitative agreement between the experimental and theoretical results allows us to determine the effective conductance and susceptance of the double dot as a function of the energies of the single-electron states. Our measurements thus present a first quantitative analysis of the complex admittance of a double quantum dot. The demonstrated technique also provides the basis for a simple and fast detection scheme for charge and spin state readout in carbon nanotubes - a material with considerable potential for spin-based quantum information processing [8–13] - without the need for a separate charge detector [14].

The device we consider is a carbon nanotube grown by chemical vapour deposition on degenerately doped Si ter-

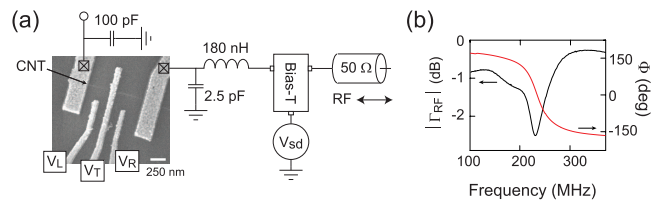


Figure 1: **(a)** (color online) Schematic of the carbon nanotube double quantum dot and resonant circuit. The device is connected to a $50\ \Omega$ transmission line for the rf reflectometry measurements. A dc signal is applied via a bias-tee. **(b)** Measured amplitude and phase response for the resonant circuit relative to the transmission line background.

minated by 300 nm SiO_2 , see Fig. 1(a). The nanotube is contacted by Au source and drain electrodes which form the outer tunnel barriers of the quantum dots. A capacitively coupled top gate, separated from the nanotube by ~ 3 nm AlO_x , is used to define a tunable coupling between the dots while two plunger gates vary the energies of the dots. The nanotube device is embedded in a resonant circuit consisting of a parasitic capacitance $C = 2.5$ pF and on-chip inductor $L = 180$ nH [15]. The circuit has a resonance frequency $f_0 \sim 236$ MHz and loaded quality factor $Q \sim 1/Z_0\sqrt{L/C} \sim 5.4$, where $Z_0 = 50\ \Omega$ is the characteristic impedance of the transmission lines, see Fig. 1(b). We note that higher quality factors ($Q \sim 30$) were readily obtained on nanotube devices grown on undoped Si and quartz substrates. A highly doped Si substrate is used here because of its convenience as a back gate.

The nanotube device is characterized by dc transport measurements and rf reflectometry in a dilution refrigerator with a base temperature $T \sim 40$ mK. The dc signal is applied via a bias-tee while the rf excitation is directed to the source electrode of the double quantum dot through the coupled port of a directional coupler, connected to the sample holder via a stainless-steel semi-rigid coaxial line, see Fig. 1(a). The reflected signal is sent back via a cryogenic preamplifier which is thermally anchored at 4 K, followed by room temperature amplification and de-

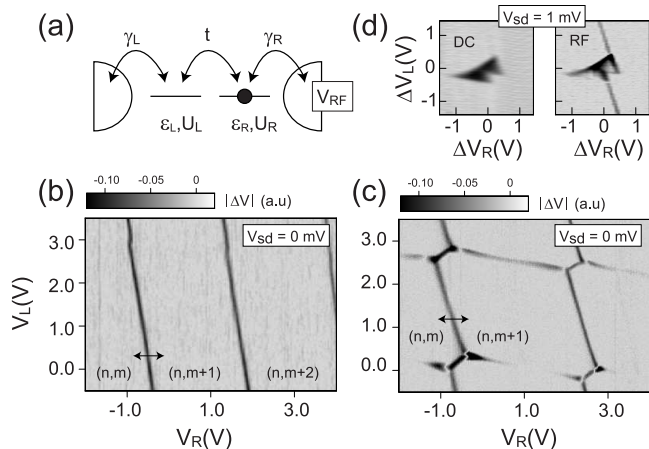


Figure 2: **(a)** Schematic of the carbon nanotube double quantum dot device. The rf signal is applied to the right electrode. **(b,c)** Demodulated response of the resonant circuit as a function of V_L and V_R . In each plot the background signal measured inside a stable charge region is subtracted. The top gate voltage is set to $V_t = 0$ V. The back gate voltages are $V_{bg} = 5$ V and $V_{bg} = -0.18$ V in (b) and (c), respectively. **(d)** Measured rf signal (right) and dc current (left) for a triple point pair in the presence of an applied bias $V_{sd} = 1$ mV. The full scale of the dc current represents 150 pA.

modulation by mixing with the reference signal. We drive the resonator at its resonant frequency with an amplitude at the double dot $V_{RF} \sim 10 \mu\text{eV}$. Depending on the energies of the quantum dots, the oscillating potential on the source electrode may induce charge transfer (tunneling) between the electrodes and the quantum dots and/or redistribution of charge between the two dots. The resulting oscillating current will generally have both out-of-phase and in-phase components with respect to the driving voltage which give rise to a resonance frequency shift and damping of the resonator. The response of the double quantum dot is thus characterized by a complex admittance which can be deduced by measuring the phase and amplitude of the reflected rf signal.

We first determine the various energy scales of the double quantum dot by measuring the dc and rf response as a function of the side-gate voltages V_L and V_R which modulate the left and right quantum dot energies, respectively, see Fig. 2. For simplicity in-phase and out-of-phase components of the rf response are shown together here (i.e. the demodulated signal is sensitive to both amplitude and phase). The nanotube device is fully tunable by the top V_t and back gate V_{bg} voltages. The stability diagram of Fig. 2(b), for example, illustrates the situation where the two quantum dots are fully decoupled: no dc current could be detected but a strong rf response is observed at charge transitions of the right quantum dot. For more positive back gate voltages, the stability diagram evolves into a honeycomb pattern that is characteristic of the double quantum dot investigated here. At

finite bias $V_{sd} = 1$ mV, bias triangles are observed at the triple points in both the dc and rf response, see Fig. 2(d), which allows us to extract the characteristic energy scales of the double quantum dot. We obtain charging energies $U_L \sim 6.5$ meV and $U_R \sim 5$ meV for the left and right quantum dots, respectively, and an inter-dot electrostatic coupling energy $U' = 0.6$ meV. The analysis also allows us to deduce the various geometric capacitances of the device [16]. We did not observe any obvious four-fold periodicity in the stability diagrams, an indication that the orbital degeneracy of the nanotubes is broken [17, 18].

To determine the complex admittance of the nanotube device we measured the in-phase and quadrature components of the reflected signal for the double quantum dot which allows us to extract the amplitude and phase information, see Fig. 3(a) and (b). The observed phase shifts $\Delta\Phi$, relative to the phase measured inside a stable charge region, are strongest at the $(n, m) - (n, m+1)$ charge transition, with a signal of about half the strength observed at the internal $(n+1, m) - (n, m+1)$ charge transition. The amplitude shifts on the other hand are concentrated around the triple points. Using standard circuit analysis [19], the measured phase signal at resonance can be related to a change in capacitance as $\Delta\Phi/\Delta C \sim 2Q/C$, where $C = 2.5$ pF for the circuit considered here. At the $(n, m) - (n, m+1)$ charge transition, for example, the measured phase shift of ~ 0.18 degrees implies $\Delta C = 0.74$ fF. Note that this is several orders of magnitude larger than the geometric capacitances of carbon nanotube quantum dots which are typically in the aF range. The amplitude modulation is related to the double dot resistance R via $\Delta|\Gamma|/|\Gamma| = 2Q^2 Z_0/R$. The measured damping $\Delta|\Gamma|/|\Gamma| \sim 0.2\%$ at the triple points therefore implies $R \sim 1.5$ M Ω which is in agreement with dc conductance measurements.

In the following we compare the experimental results with a theoretical model of the device, the full results of which are shown in Fig. 3(c) and (d) which show the real (R_{eff}^{-1}) and imaginary (C_{eff}) part of the admittance as a function of the energies of the quantum dots' single-electron states. We model the the admittance measured at the source electrode using a master equation approach similar to Ref. [4]. We take into account all relevant many body states, i.e. for Fig. 3(c) and (d) the empty state and all one and two electron states. For a given set of gate voltages V_L, V_R we obtain the steady state density matrix at zero bias. We then calculate the current flowing into the source electrode as a linear response to a periodic driving of the source potential. This enables us to deduce the double quantum dot admittance at the source electrode. We assume that the driving frequency is too small to induce transitions between quantum dot eigenstates and we therefore treat the perturbation as adiabatic. The current into the source has two contributions: the particle current due to tunneling from the source to the left dot and the displacement current induced on the

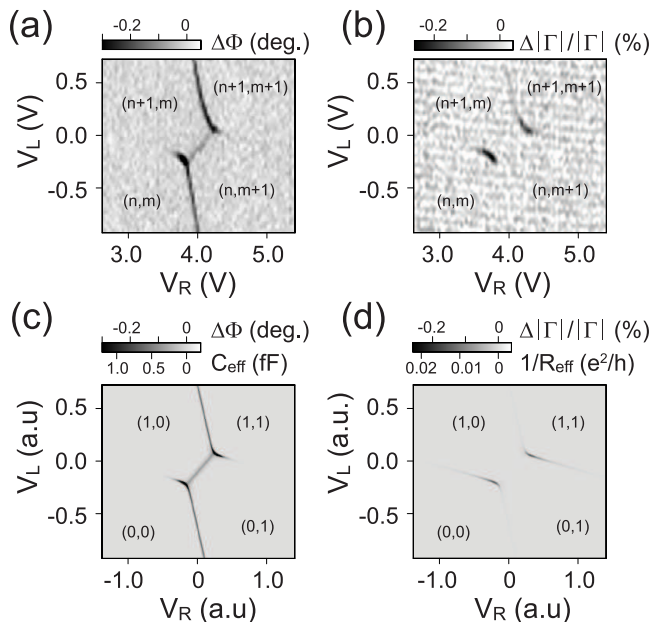


Figure 3: (a) Measured phase shift of the carbon nanotube double quantum dot device. (b) Measured amplitude response. (c) Calculated effective capacitance and phase shift of the double quantum dot. The parameters used for the model calculations are $T = 80$ mK, $U' = 0.6$ meV, $t = 40$ μ eV, $\omega_0 = 1.2$ GHz, $\gamma_L = 0.15\gamma_R$. (d) Calculated conductance and damping for the same parameters as used in (c).

source capacitance by the tunneling induced redistribution of charges on the quantum dot. We include spin relaxation as well as phonon assisted tunneling between the left and the right dot. Overall, we obtain good agreement with the experimental results as demonstrated by Fig. 3.

For a physical understanding of the results (and the model) it is instructive to consider several limiting cases. Let us first consider transitions between (n, m) and $(n, m + 1)$ charge states such that direct charge transfer between the two electrodes (a dc current) and internal transitions of the double quantum dot can be neglected. An oscillating potential $V_{RF}(t)$ on the right electrode modulates the energy difference $\delta\epsilon(t)$ between the right quantum dot states and the Fermi energy of the lead as $\delta\epsilon(t) = \epsilon_0 - e\alpha V_{RF}(t)$, where ϵ_0 is an offset, tunable with the plunger gates. The constant $e\alpha$ converts between voltage and energy and its value depends on the various geometric capacitances of the device [16]. As a result of the oscillating potential, charge moves back and forth between the right electrode and right quantum dot. Depending on the ratio of the tunnel rate γ_R and angular driving frequency ω_0 , the induced current has both in-phase and out-of-phase components with respect to the voltage which can be expressed as a complex admittance $Y(\omega_0) = R_{eff}^{-1} + j\omega_0 C_{eff}$. In the incoherent limit, i.e. for

$h\gamma_R \ll k_B T$ the terms are given by [5]:

$$R_{eff} = \frac{4k_B T}{e^2 \alpha^2 \gamma_R} \left(1 + \frac{\gamma_R^2}{\omega_0^2} \right) \quad (1)$$

$$C_{eff} = \frac{e^2 \alpha^2}{4k_B T} \frac{1}{1 + \frac{\omega_0^2}{\gamma_R^2}} \quad (2)$$

As expressed by Eqs. (1) and (2), both the conductance and capacitance are dependent on the ratio of the tunnel coupling and angular driving frequency. In the transparent limit ($\gamma \gg \omega_0$), the effective capacitance can be approximated by $C_{eff} \approx e^2 \alpha^2 / 4k_B T$. The conductance has a vanishing contribution, i.e. $R_{eff}^{-1} \rightarrow 0$, in both the transparent and opaque limit. This can be understood intuitively as for very large γ electrons will tunnel on the quantum dot as soon as this is energetically possible and no energy is dissipated in the process. In the opaque limit, tunneling occurs out of equilibrium. However, as the probability of a tunnel event on the timescale of the driving frequency vanishes for weak coupling, no energy is dissipated either. Damping is therefore strongest in the intermediate regime where $\gamma \sim \omega$, as recently observed for single-electron tunneling devices coupled to electrical [20, 21] and mechanical [22] resonators.

We can compare these predictions with the experimental data obtained on the carbon nanotube double quantum dot. Using $\alpha \approx 0.35$, as determined from dc transport experiments, we obtain quantitative agreement between the experiment ($\Delta\Phi \sim 0.18$ degrees) and the change in capacitance predicted by Eq. 2 for the (n, m) - $(n, m + 1)$ transition, if we assume an effective electron temperature $T \sim 80$ mK [23]. This is somewhat larger than the base temperature of the dilution fridge, most likely due to heat loading of the device by the coaxial cables. The estimate of the effective capacitance at the (n, m) - $(n + 1, m)$ transition, i.e. due to charge transfer between the left lead and left dot also follows Eq. 2. However in this case, the prefactor is much smaller $\alpha \sim 0.05$ reflecting the weak coupling between the left quantum dot and the right electrode at which the rf signal is applied. Since the expected phase shift $\propto \alpha^2$ the response along this line is too weak to be detected. We observe a very weak amplitude modulation along the (n, m) - $(n, m + 1)$ charge transition, $\Delta|\Gamma|/|\Gamma| \sim 0.05\%$, most clearly observed in the top half of Fig. 3(b). This is consistent with damping due to out-of-equilibrium tunneling and in agreement with the theoretical calculations of the effective conductance shown in Fig. 3(d). The fact that the signal is rather weak implies that $\gamma_R \gtrsim \omega_0$ in our device. Stronger damping is observed at the triple points where the behavior of the device is similar to that of the conventional rf single-electron transistor [24].

Of particular interest is the phase signal along the polarization line which reflects the movement of electrons

between the quantum dots, i.e. transitions between the $(n+1, m)$ and $(n, m+1)$ charge states. In this case, the amplitude and width of the signal is not set by temperature but the tunnel coupling t . More precisely, it has been predicted [4] that, $C_{eff} = e^2 \beta^2 / 4t$, where here $\beta \sim 0.6$ converts between V_{RF} and detuning $\epsilon_L - \epsilon_R$. The predictions can be directly verified with our experiments. The tunnel coupling can be deduced from the stability diagram [25], yielding $t \sim 40 \mu\text{eV}$, and the estimate for $C_{eff} \approx 0.46 \text{ fF}$ therefore has no free parameters. This result is in excellent agreement with the experimental data of Fig. 3(a) where we measure a phase shift of ~ 0.11 degrees, roughly a factor ~ 2 smaller than that observed at the $(n, m) - (n+1, m)$ transition, as also seen in the model calculation of Fig. 3(c).

We note that we did not observe spin blockade in dc transport experiments on the carbon nanotube double quantum dot studied here and the effect is therefore not taken into account in the analysis. Nevertheless, spin blockade has been observed previously in carbon nanotubes [10, 11, 13]. In the spin blockade regime, transitions between a (1,1) and (0,2) charge state directly depend on whether the (1,1) state is a singlet or triplet. Since the (0,2) charge state is a singlet by virtue of the Pauli principle the (1,1) triplet state will be a blocked state which is reflected in the admittance [4]. Measurements of the admittance of a carbon nanotube double quantum dot as demonstrated here can therefore also be used for spin state readout [7].

In conclusion, we have measured the complex admittance of a carbon nanotube double quantum using rf reflectometry. The results are in quantitative agreement with a theoretical model of the device of which several limiting cases are discussed in detail. The demonstrated technique is of particular interest as a tool for fast and sensitive charge and spin state readout of carbon nanotube quantum dots. A further interesting possibility is to extend the measurement to the coherent limit where the nanotubes are more strongly coupled to the leads. This should allow the observation of a quantized charge relaxation resistance [5] and possible deviations thereof in long nanotubes for which interactions (Luttinger liquid physics) become important [26, 27].

We thank David Cobden and Jiang Wei for the carbon nanotube growth and Andrew Ferguson for useful discussion. This work was supported by the Newton Trust and the Royal Society (M.R.B.).

* Current address: Department of Physics, Princeton University, Princeton, NJ 08544, USA

† Electronic address: mrb51@cam.ac.uk

[1] M. Büttiker, A. Prêtre, and H. Thomas, Phys. Rev. Lett. **70**, 4114 (1993).

- [2] A. Prêtre, H. Thomas, and M. Büttiker, Phys. Rev. B **54**, 8130 (1996).
- [3] D. Loss and D.P. DiVincenzo, Phys. Rev. A **57**, 120 (1998).
- [4] A. Cottet, C. Mora, and T. Kontos, Phys. Rev. B **83**, 121311 (2011).
- [5] J. Gabelli, G. Fève, J.-M. Berroer, B. Plaçais, A. Cavanaugh, B. Etienne, Y. Jin, and D.C. Glattli, Science **313**, 499 (2006).
- [6] M.R. Delbecq, V. Schmitt, F.D. Parmentier, N. Roch, J.J. Viennot, G. Fève, B. Huard, C. Mora, A. Cottet, and T. Kontos, arXiv:1108.4371.
- [7] K.D. Petersson, C.G. Smith, D. Anderson, P. Atkinson, G.A.C. Jones, and D.A. Ritchie, Nano Lett. **10**, 2789 (2010).
- [8] F. Kuemmeth, S. Ilani, D.C. Ralph, and P.L. McEuen, Nature (London) **452**, 448 (2008).
- [9] C. Galland and A. Imamoğlu, Phys. Rev. Lett. **101**, 157404 (2008).
- [10] H.O.H. Churchill, A.J. Bestwick, J.W. Harlow, F. Kuemmeth, D. Marcos, C.H. Stwertka, S.K. Watson, and C.M. Marcus, Nature Phys. **5**, 321 (2009).
- [11] H.O.H. Churchill, F. Kuemmeth, J.W. Harlow, A.J. Bestwick, E.I. Rashba, K. Flensberg, C.H. Stwertka, T. Taychatanapat, S.K. Watson, and C.M. Marcus, Phys. Rev. Lett. **102**, 166802 (2009).
- [12] T.S. Jespersen, K. Grove-Rasmussen, J. Paaske, K. Muraki, T. Fujisawa, J. Nygård, and K. Flensberg, Nature Phys. **7**, 348 (2011).
- [13] S.J. Chorley, G. Giavaras, J. Wabnig, G.A.C. Jones, C.G. Smith, G.A.D. Briggs, and M.R. Buitelaar, Phys. Rev. Lett. **106**, 206801 (2011).
- [14] M.J. Biercuk, D.J. Reilly, T.M. Buehler, V.C. Chan, J.M. Chow, R.G. Clark, and C.M. Marcus, Phys. Rev. B **73**, 201402(R) (2006).
- [15] The main component of the capacitance is the parallel plate capacitor formed by the bond pad and Si back gate.
- [16] W.G. van der Wiel, S. De Franceschi, J.M. Elzerman, T. Fujisawa, S. Tarucha, and L.P. Kouwenhoven, Rev. Mod. Phys. **75**, 1 (2002).
- [17] W.J. Liang, M. Bockrath, and H. Park, Phys. Rev. Lett. **88**, 126801 (2002).
- [18] M.R. Buitelaar, A. Bachtold, T. Nussbaumer, M. Iqbal and C. Schönenberger, Phys. Rev. Lett. **88**, 156801 (2002).
- [19] D.M. Pozar, *Microwave Engineering*, 3rd ed. (Wiley, New York, 2005).
- [20] F. Persson, C.M. Wilson, M. Sandberg, G. Johansson, and P. Delsing, Nano Lett. **10**, 953 (2010).
- [21] C. Ciccarelli and A.J. Ferguson, arXiv:1108.3463.
- [22] Z. Jun, M. Brink, P.L. McEuen, Nano Lett. **8**, 2399 (2008).
- [23] For this temperature $k_B T / h \gamma_R \sim 2$.
- [24] R.J. Schoelkopf, P. Wahlgren, A.A. Kozhevnikov, P. Delsing, and D.E. Prober, Science **280**, 1238 (1998).
- [25] M.R. Gräber, W.A. Coish, C. Hoffmann, M. Weiss, J. Furer, S. Oberholzer, D. Loss, and C. Schönenberger, Phys. Rev. B **74**, 075427 (2006).
- [26] Y. Hamamoto, T. Jonckheere, T. Kato, and T. Martin, Phys. Rev. B **81**, 153305 (2010).
- [27] P.J. Burke, IEEE T. Nanotechnol. **1**, 129 (2002).